Locations for the best lidar view of mid-level and high clouds

Matthias Tesche[1] and Vincent Noel[2]

[1]Leipzig Institute for Meteorology, Leipzig University, Stephanstraße 3, 04103 Leipzig, Germany
[2]Laboratoire d'Aérologie, CNRS/UPS, Observatoire Midi-Pyrénées, 14 avenue Edouard Belin, Toulouse, France

Correspondence: Matthias Tesche (matthias.tesche@uni-leipzig.de)

Abstract.

Mid-level altocumulus clouds (Ac) and high cirrus clouds (Ci) can be considered as natural laboratories for studying cloud glaciation in the atmosphere. While their altitude makes them difficult to access with in-situ instruments, they can be conveniently observed from the ground with active remote-sensing instruments such as lidar and radar. However, active remote sensing of Ac and Ci at visible wavelengths with lidar requires a clear line of sight between the instrument and the target cloud. It is therefore advisable to carefully assess potential locations for deploying ground-based lidar instruments in field experiments or for long-term observations that are focused on mid- or high-level clouds. Here, observations of clouds with two spaceborne lidars are used to assess where ground-based lidar measurements of mid- and high-level clouds are least affected by the light-attenuating effect of low-level clouds. It is found that cirrus can be best observed in the tropics, the Tibetan plateau, the western part of North America, the Atacama region, the southern tip of South America, Greenland, Antarctica, and parts of western Europe. For the observation of altocumulus, a ground-based lidar is best placed at Greenland, Antarctica, the western flank of the Andes and Rocky Mountains, the Amazon, central Asia, Siberia, western Australia, or the southern half of Africa.

1 Introduction

Clouds have a strongly modulating effect on the radiative transport of energy in the atmosphere. They affect planetary albedo and, thus, the amount of solar radiation arriving at the ground. Because it is hard to get to cloud level for direct measurements (Baumgardner et al., 2017), studies of cloud properties often resort to remote-sensing observations (Buehl et al., 2017), particularly to active remote sensing with lidar or cloud radar.

Since the beginning of atmospheric remote sensing with lidar, cirrus (Ci) clouds (Heymsfield et al., 2017) have been a focus of observational efforts (Platt, 1973, 1979; Sassen and Cho, 1992; Sassen and Campbell, 2001). Lidar has turned out to be the best option for long-term monitoring of cirrus occurrence as well as their optical and geometrical properties (Comstock et al., 2002; Seifert et al., 2007; Dupont et al., 2010; Hoareau et al., 2013; Kienast-Sjögren et al., 2016). In addition, observations of cirrus clouds have been used to demonstrate new lidar measurement techniques (Ansmann et al., 1992) and to validate the performance of spaceborne lidar instruments (Yorks et al., 2011).

Altocumulus (Ac) clouds (Gedzelman, 1988; Korolev et al., 2017) are often mixed-phase clouds that consist predominantly of supercooled liquid water droplets and, hence, are highly susceptible to the effect of ice-nucleating particles (INPs). They, therefore, mark a natural laboratory for studies of heterogeneous glaciation in environments where efficient INPs are present.

Polarization lidar measurements can be used to investigate the effect of mineral dust (Ansmann et al., 2005, 2008, 2009, 2019; Seifert et al., 2010), volcanic ash (Seifert et al., 2011), or other aerosol particle types (Kanitz et al., 2011; Seifert et al., 2015; Cheng and Yi, 2020; Radenz et al., 2021; Yi et al., 2021) acting as INP in the heterogeneous glaciation of altocumulus clouds.

30 However, active remote sensing of mid-level and high clouds with lidar at visible wavelengths requires a clear line of sight between the instrument and the target cloud. Particularly low-level liquid water clouds, that attenuate the emitted laser light close to the ground are a major obstacle for long-term observations of mid- and high-level clouds. It is therefore advisable to carefully assess potential locations regarding the likelihood of measurements being hindered by low-level clouds if a lidar was to be deployed for a field experiment or long-term observations that focus on mid- or high-level clouds.

35 Here, spaceborne lidar observations of clouds, for which the light-attenuation of low-level clouds has no effect on the detection of mid-level and high clouds, are used to assess where ground-based lidar measurements of altocumulus and cirrus are least affected by low-level cloudiness. The same methodology has already been used for finding locations at which tropospheric clouds are likely to minimally interfere with observation of Polar Tropospheric Clouds with ground-based lidar (Tesche et al., 2021). The used data and methodology are presented in Section 2. The results are shown and discussed in Section 3. The paper

40 concludes with a summary in Section 4.

2 Data and methodology

2.1 CALIPSO cloud profile data

The Cloud-Aerosol Lidar with Orthogonal Polarization (CALIOP) lidar aboard the CALIPSO satellite (Winker et al., 2009) is an elastic-backscatter lidar that operates at 532 and 1064 nm with co- and cross-polarized channels at the former wavelength.

45 Since June 2006, CALIOP has become an invaluable tool for monitoring the three-dimensional distribution of aerosols and clouds in the troposphere and stratosphere (Winker et al., 2013; Pitts et al., 2018). CALIPSO lidar measurements have been used to study the occurrence and properties of clouds (Hong and Liu, 2015), often in combination with measurements from other instruments in the A-Train satellite constellation, such as radiometers or cloud radar.

For this study, information on the extent and type of tropospheric clouds with a resolution of 5 km along the CALIPSO

50 ground track and 30-m height bins below 8.2 km height (60-m height bins between 8.2 and 20.2 km height) is taken from the CALIPSO Level 2 Version 4.20 Cloud Profile product (05kmCPro.v4.20). The extracted parameters are time, latitude, longitude, the day-night flag, and the cloud type as provided in the Vertical Feature Mask (Liu et al., 2009). The data considered here cover the years 2007 to 2021. Table 1 gives an overview of the number of CALIPSO lidar profiles included in this study.

2.2 CATS cloud profile data

55 Based on the International Space Station (ISS), the Cloud-Aerosol Transport System (CATS, McGill et al. 2015) performed elastic-backscatter measurements at 1064 nm from February 2015 to October 2017 (Pauly et al., 2019). In contrast to CALIPSO, the orbit of the ISS has an inclination of 51.6° and is not sun-synchronous. Therefore, CATS observations are restricted to

latitudes lower than 51°, but allow for covering different times of the day. This latter capability is used here to assess the representativeness of cloud observations at the fixed CALIPSO equator pass times of 0130 and 1330 local time.

60   Two Level 2 CATS-ISS products are used to document the diurnal variability of clouds. The first is the L2O Profile product (05kmPro.v3.01, Yorks et al. 2016a) which documents profiles of various atmospheric properties at 60 m vertical resolution in 5-km intervals along the ISS ground track. These profiles are derived mainly from the attenuated backscatter coefficient measured at 1064 nm. Profiles of feature type (Feature_Type_Fore_FOV, 1 indicating a cloud) and of cloud phase (Cloud_Phase_Fore_FOV, 3 indicating ice) for a given time, latitude, and longitude (Yorks et al., 2016b) are used to

65   derive a mask for ice clouds. From the L2O Layer product (05kmLay.v3.01), which documents layer-integrated properties for atmospheric features found in profiles of 1064-nm attenuated backscatter, the feature type (Feature_Type_Fore_FOV, 1 indicating a cloud), base and top altitude and pressure for each detected layer, and the profile opacity indicator (Percent_Opacity_Fore_FOV) are used to document the presence of altocumulus clouds. Such clouds are identified following the same criteria as in the CALIPSO scene classification (Liu et al., 2005): a non-opaque cloud layer with a top pressure be-

70   tween 440 and 680 hPa. For both products, it is required that the quality scores, that range between 0 and 10, have to be larger than 5 for cloud identification.

A comparison between the fractions of cirrus and altocumulus clouds as inferred from the data sets of CALIPSO and CATS following the approaches described above is presented in the Appendix.

2.3   Determination of cloudiness

75   The CALIPSO retrieval separates between eight cloud types (Liu et al., 2009): (i) low overcast, transparent; (ii) low overcast, opaque; (iii) transition stratocumulus; (iv) low, broken cumulus; (v) altocumulus (transparent); (vi) altostratus (opaque); (vii) cirrus (transparent); and (viii) deep convective (opaque). For each profile, the number of height bins in which a certain cloud types was identified is summed up. The simplified data set is then used to assess if a certain cloud type is present (total count per profile larger zero) or not.

80   In the analysis, two scenarios are considered. In the first setup, the data set is screened for cloudy profiles that depict cirrus in the absence of opaque low- and mid-level clouds. These cases represent conditions under which cirrus could be detected by a ground-based lidar without the interference of lower clouds. This scenario will be referred to as isolated cirrus. The second setup refers to the possibility of detecting mid-level clouds with a ground-based lidar by screening the data set for profiles in which transparent altocumulus is identified without the presence of any of the four low-level cloud types below. Underlying

85   low-level clouds need to be detected to achieve the aim of this study. Hence, opaque altocumulus is not included in the analysis of mid-level clouds.

The number of thus selected profiles is mapped on a grid of 2.50° longitude by 1.25° latitude to assess the occurrence rate of conditions for which a ground-based instrument could observe mid-level and high clouds without attenuation of the laser beam by clouds at lower levels.

90   The day-night flag is used to assess changes in cloud occurrence for CALIPSO overpasses during day and night. The annual variation is studied by compiling maps for the months December, January, February (DJF); March, April, May (MAM); June,

July, August (JJA); and September, October, November (SON). The number of profiles in the different categories is given in Table 1 to provide an overview of the considered volume of data.

3 Results

3.1 Cirrus clouds

An overview of the occurrence of isolated cirrus as identified from 15 years of CALIPSO lidar measurements is provided in Figure 1. The land regions with the highest occurrence frequency of 0.5 or larger are the Tibetan plateau, north-eastern Africa (Chad, Egypt, Libya, Sudan), Saharan Africa, California, northern Chile, and eastern Antarctica. Over water, the largest occurrence frequencies are found over the Caribbean, the western Indian Ocean, as well as in two bands north and south of the intertropical convergence zone (ITCZ). The distribution in Figure 1a changes considerably if the number of CALIPSO profiles that show isolated cirrus is normalized by the number of cirrus-containing cloudy profiles (Figure 1b) rather than all cloudy CALIPSO profiles (Figure 1a). The absolute number of cirrus-containing CALIPSO profiles in Figure 1c shows that regions with high coverage of isolated cirrus in Figure 1a and b, such as north-eastern Africa and California, actually feature a rather low occurrence rate of cirrus-containing CALIPSO profiles. Combining the information in Figure 1 reveals that the land sites with the best temporal coverage for observing isolated cirrus clouds from the ground have to feature (i) a large ratio of cirrus observations in the absence of low- and mid-level clouds with (ii) a high occurrence rate of cirrus-containing profiles.

Differences between day and night are summarized in Figure 2. The differences are likely related to the combined effect of diurnal variability and variations in detection sensitivity. The increased detection sensitivity during the night (related to the absence of background noise from scattered sunlight) generally leads to an increase in the number of cirrus-containing cloudy profiles south of about 55°N, while the opposite is the case at higher latitudes (not shown). Nevertheless, the general patterns of cirrus occurrence for CALIPSO observations during day and night do not differ from those in figure Figure 1a.

The seasonal variation of the occurrence of isolated cirrus clouds is presented in Figure 3. The region with the highest occurrence rate of isolated cirrus clouds is northern Africa during boreal winter. Other regions of pronounced seasonal variation are the west coast of North America, Chile, the southern tip of Africa, the Arabian peninsula, the Indian Ocean and the Indian subcontinent, Tibet and western China, the maritime continent, and the equatorial Pacific Ocean. In contrast to these regions, seasonal variations at the poles are the result of the effect of polar night and day. This can also be seen from comparing Figures 1 and 2.

3.2 Mid-level clouds

Occurrence rates of transparent mid-level clouds that would be detectable with a ground-based lidar from 15 years of CALIPSO data are presented in Figure 4. The land regions with the highest fraction of CALIPSO profiles that contain transparent altocumulus clouds without low-level clouds below are the Greenland ice sheet, eastern Antarctica, the western flanks of the Rocky Mountains and Andes, western Australia, southern Africa and the Horn of Africa, large parts of the Middle East, and the area

around the Himalayas. Figures 4b and c reveal that cloudy profiles containing transparent altocumulus are dominant over the continents and the equatorial oceans. A similar finding is presented in Bourgeois et al. (2016). In contrast, transparent altocumulus generally occurs less frequently over mid-latitude oceans and the stratocumulus decks to the west of the continents, though aircraft measurements have shown that the occurrence rate of thin mid-level clouds is non-negligible in these regions (Adebiyi et al., 2020).

The day-night contrast for altocumulus clouds in Figure 5 is more pronounced than the one for isolated cirrus in Figure 2 with a larger occurrence rate of continental transparent altocumulus clouds without low-level clouds underneath during daytime. This is particularly visible over western North America, southern and eastern Africa, eastern Antarctica, and western Australia. A slight increase in the occurrence rate is found over the equatorial oceans during the night, again likely as a result of increased detection sensitivity in the absence of the solar background. The occurrence frequency is lowest over the regions of dense stratocumulus decks to the west of the continents.

Figure 6 reveals that some regions show a considerable change in the occurrence frequency of transparent altocumulus over the year. This seasonal variation would need to be considered in the choice of location for ground-based lidar observations of mid-level clouds and in the interpretation of the collected data. For instance, ground-based lidar measurements of transparent altocumulus clouds located in northern Africa, the Middle East, or at the west coast of North America are likely to give the best yield in observations during summer, while the occurrence frequency of those clouds is considerably lower during other seasons. In contrast, the opposite is found for Eastern Africa. Occurrence frequencies are relatively constant over the southern part of Africa, the Atacama region, Greenland, western Australia, and central Asia.

3.3 Diurnal variability

An extensive comparison of the findings from observations with the CATS and CALIPSO lidars is provided in the Appendix. Here, the capability of CATS to cover the diurnal variability in cloudiness in the latitude band from 51°S to 51°N (Noel et al., 2018) is used to evaluate the representativeness of the CALIPSO lidar observations at 0130 and 1330 local time for drawing conclusions regarding the most suitable regions for observing mid-level and high clouds with ground-based lidar instruments. A comparison of the occurrence of high- and mid-level clouds in CALIPSO observations that cover just the CATS time period versus the 15 full years considered in Figures 1-6 reveals no change in the observed patterns (not shown). We hence conclude that the findings of this section can be generalized to CALIPSO observations that don't fall within the time during which CATS has been active.

Figure 7 presents the analysis of CATS observations of isolated ice clouds over its full period of operation from March 2015 to October 2017. Though compiled with a coarser resolution, the occurrence-frequency map in Figure 7a can be compared directly to the CALIPSO observations in Figure 1a. Data from both instruments give a very similar global distribution of isolated cirrus clouds with clear maxima of occurrence over northern Africa and the Tibetan plateau. Therefore, it is reasonable to make use of both time series for a more comprehensive analysis of the best locations for observing mid-level and high clouds with ground-based lidar.

The anomaly in the diurnal variation of the zonal mean occurrence rate of isolated ice clouds over all surfaces in Figure 7b reveals that noontime measurements in the northern hemisphere show lower values than the daily average of CATS observations, while the opposite is the case for evening measurements. A much smaller variation from the daily average is found in the first six to nine hours of a day. A similar picture is found when looking at zonal mean values for different seasons (not shown). The diurnal variation in zonal bands of 20° is shown in Figure 7d. Over all surfaces, measurements in the tropics from 30°S to 30°N show the largest anomaly at noon and in the evening. Smaller variations are found at latitudes larger than 30°. All zonal bands show mean values varying around zero until 0600 local time. Figure 7c shows that the diurnal variation is intensified when considering only data over land, which are the areas where a ground-based lidar would be placed. In that case, a stronger negative anomaly is found around noon compared to the data over all surfaces in Figure 7b, while a positive anomaly extends from 1800 to 0600 local time, though weakening after midnight. This is corroborated by the zonal means over land in Figure 7d, which also reveal the smallest anomaly during the morning hours. From this investigation of diurnal variation and the magnitude of the anomaly during day and night, it can be concluded that CALIPSO night time observations at 0130 local time might be more representative for an objective assessment of the ideal regions for observing mid-level and high clouds with ground-based lidar instruments compared to daytime observations at 1330 local time.

The results of an analogous investigation for transparent altocumulus clouds are presented in Figure 8. Again, the distribution of isolated altocumulus clouds from CATS observations resembles that derived from the CALIPSO time series in Figure 4a. However, the smaller volume of the CATS data set in combination with the coarser resolution of the spatial gridding leads to a weaker contrast in altocumulus occurrence in Figure 8a compared to the CALIPSO data in Figure 4a. The anomaly in the diurnal variation of the zonal mean occurrence rate of isolated altocumulus is much weaker than for cirrus for observations over all surfaces as well as land only. In fact, the anomaly is negligible when considering all surfaces (Figure 8b and d). Considering only data over land shows a weak positive anomaly around noon and an even weaker negative anomaly between 1800 and 0600 local time (Figure 8c). Hence, CALIPSO observations at 0130 local time should be representative for the better part of a day.

3.4 Placing a ground-based lidar for observations of high and mid-level clouds

The findings of this study are summarized in Figure 9. Additional maps with higher temporal resolution as reference for short-term instrument deployment are provided in Figures A5-A8. The combination of (i) the ratio of CALIPSO profiles containing either cirrus clouds in the absence of opaque low- and mid-level clouds or transparent altocumulus in the absence of low-level clouds versus all cloudy profiles (Figures 1a and 4a) with (ii) the normalized number of such CALIPSO profiles per grid box (Figures 1c and 4c) is used to identify those land regions where measurements with a ground-based lidar are most likely to yield the highest possible observation rate for studying mid-level and high clouds.

Unsurprisingly, cirrus clouds are best observed in the tropics with particularly suitable conditions for ground-based lidar measurements at the northern coast of South America, equatorial Africa, the southern tip of the Indian subcontinent, and the maritime continent. Cirrus observations with lidar in these regions have been performed, for instance, in Niger (Protat et al., 2010), in southern India (Pandit et al., 2015), at the Maldives (Seifert et al., 2007), and at Nauru (Comstock et al., 2002). Further favourable regions are the Tibetan plateau (Dai et al., 2019; He et al., 2013) and western China, western

North America (Sassen and Campbell, 2001; Sassen and Benson, 2001), Florida and the Caribbean (Haarig et al., 2016), the Atacama region, the southern tip of South America (Barja Gonzalez et al., 2020), the Amazon rain forest (Gouveia et al., 2017), Antarctica (Alexander and Klekociuk, 2021), and Greenland (Lacour et al., 2018), where semi-transparent clouds were found to potentially enhance ice sheet melting (Bennartz et al., 2013; Solomon et al., 2017). Less ideal conditions are met over Europe (Giannakaki et al., 2007; Kienast-Sjögren et al., 2016) and most of Asia. The worst regions are the Canadian Arctic, the northern parts of Europe and Asia, the Middle East, southern Africa, and most of Australia. Nevertheless, studies have been published based on measurements at those regions as well (e.g. Platt 1973, Protat et al. 2010).

The preferential regions for observing mid-level clouds with ground-based lidar are shown in Figure 9b. These turn out to be more confined compared to the ones for cirrus in Figure 9a. The regions that stick out are the Greenland plateau and Antarctica (Del Guasta et al., 1993), where the topography is too high to have low-level clouds as an obstacle for lidar measurements. At low and mid-latitudes, advantageous observational conditions prevail at the western flanks of the Rocky Mountain (Sassen, 2002) and Andes mountain ranges (Kanitz et al., 2011; Jimenez et al., 2020), over the Amazon, western Australia (Protat et al., 2011), southern and eastern Africa, the Gulf region, the fringe of the Tibetan plateau, and central Asia. The regions indicated in Figure 9b mark those for which a ground-based lidar is likely to give the best return rate in terms of observing altocumulus clouds. This is particularly important for short-term deployments such as field experiments which typically extend over a period of a few weeks to months. Alternatively, long-term measurements are the best option for collecting a volume of data that is sufficient to allow for identifying specific case studies as well as for enabling a statistical analysis of the observed altocumulus clouds – even in regions that are not emphasised in Figure 9b, such as central Europe (Ansmann et al., 2005; Seifert et al., 2010; Schmidt et al., 2015).

Figures A5-A8 provide seasonally and monthly resolved displays of the data in Figure 9. The figures reflect the annual variation of observational conditions for consideration when planning the deployment of lidar instruments for observing mid-level or high clouds during dedicated field experiments or shorter-term measurement campaigns.

4 Summary and conclusions

Fifteen years of measurements from the polar-orbiting CALIPSO lidar have been used in combination with 32 months of measurements from the CATS lidar aboard the International Space Station between March 2015 and October 2017 to investigate the global distribution of cloud scenarios that support observations of mid- and high-level clouds with ground-based lidar instruments. The CALIPSO cloud mask was used to select profiles in which

1. cirrus clouds are observed in the absence of low-level clouds and opaque altocumulus underneath, and

2. transparent altocumulus is observed in the absence of low-level clouds underneath,

as an analogue for conditions under which a ground-based lidar could be used for unperturbed observations of high- and mid-level clouds, respectively.

The fixed CALIPSO overpass times at 0130 and 1330 local time inhibit an assessment of the diurnal variation in cloudiness. Hence, observations with the CATS lidar have been used to investigate the representativeness of the CALIPSO cloud sampling. While the CATS data set flags water and ice clouds, additional screening is needed to identify cloud types such as altocumulus and cirrus as provided in the CALIPSO data set. Scenarios that are comparable to the ones selected from the CALIPSO observations have been compiled by screening the CATS data set for the occurrence of cloud ice and for the location of cloud base and top heights.

The analysis of the data sets from the two spaceborne lidars shows a remarkable resemblance in the regional and vertical distribution of isolated cirrus and altocumulus clouds despite the different approaches to extract the corresponding information from the two data sets. The diurnal variation of cloud occurrence from the CATS data set leads to the conclusion that CALIPSO observations at 0130 local time are representative for the better part of the day, while the period of largest anomaly is covered by the overpass at 1330 local time. Generally, diurnal anomalies in cloud occurrence are (i) stronger over land compared to over all surfaces and (ii) stronger for isolated cirrus clouds compared to isolated altocumulus clouds. The ratio of occurrence of the two cloud types versus all cloudy profiles per grid box in combination with the absolute number of profiles in a corresponding grid box is used to identify those regions for which a ground-based lidar is likely to encounter the best balance between the occurrence of the desired cloud types and the prevalence of favourable conditions to actually observe these clouds, i.e. the absence of strongly light-attenuating clouds below the target cloud.

This information is particularly vital in the planning of deploying lidar instruments in the framework of field experiments or measurement campaigns. Such deployments generally last between a few weeks to several months, and their success relies strongly on finding atmospheric conditions that meet the desired research objectives to allow for addressing related science questions. From the approach used in this study, it is found that the best regions for lidar measurements of cirrus clouds are the tropics, the Tibetan plateau, the western part of North America, the Atacama region, the southern tip of South America, Greenland, Antarctica, and parts of western Europe. For the observation of altocumulus clouds, a ground-based lidar is best placed on Greenland, Antarctica, the western flank of the Andes and Rocky Mountains, the Amazon, central Asia, Siberia, western Australia, or the southern half of Africa. The seasonally and monthly resolved view of advantageous conditions for observing mid-level and high clouds with ground-based lidar reveals a strong annual variation for some of the regions identified above that should be considered in the planning of shorter-term lidar deployments. Finally, it should be emphasized that the regions identified here provide the best gain of a lidar deployment. However, this advantage for short-term deployments can be compensated by increasing the length of a lidar operating at a certain site, as this increases the likelihood of meeting the desired atmospheric conditions for observing a targeted cloud type.

Data availability. All spaceborne lidar data used in this study are openly available, e.g. through the ICARE Data and Services Center at https://www.icare.univ-lille.fr/. More specifically, the CALIPSO Cloud profile data (CALIPSO Cloud Profile product, 2022) used in this study are located at https://www.icare.univ-lille.fr/data-access/data-archive-access/?dir=CALIOP/05kmCPro.v4.20/ while the CATS data (CATS Layer product, 2022; CATS Profile product, 2022) can be found at https://www.icare.univ-lille.fr/data-access/data-archive-access/?dir=

Appendix A: Comparability of CALIPSO and CATS observations of the fraction of high- and mid-level clouds

The consistency of observations with the CALIPSO and CATS lidars is investigated for the time period from March 2015 to October 2017, i.e. the period of CATS operation. For this, CATS observations of ice and mid-level clouds collected in a time period of ± 1 h around the CALIPSO observations at 0130 and 1330 local time are used to derive cloud fraction (i) in grid boxes of $5°$ by $5°$, (ii) as latitudinal and longitudinal averages, and (iii) in the form of height profiles for comparison with CALIPSO observations. Note that the temporal constraint leads to a much lower number of CATS profiles compared to the CALIPSO observations, and thus more noise in the CATS data.

A1 Cirrus clouds

Figure A1 compares the spatial distribution of the occurrence frequency of cirrus clouds as seen by CALIPSO and CATS. Both data sets agree in their main features, i.e. maxima of ice-cloud fraction over the tropics, regions of low ice-cloud fraction in bands around $30°N$ and $30°N$, and an increase in ice-cloud fraction towards higher latitudes from there. This agreement is confirmed when considering latitudinal and longitudinal averages (not shown). The CATS and CALIPSO data sets agree in the magnitude of latitudinally averaged ice-cloud fraction with the largest deviation of about 0.05 in the band at $25°S$; an effect that might be resulting from the noise in the CATS data. The longitudinally averaged ice-cloud fraction shows bands with a larger deviation between the two data sets (from $150°W$ to $120°W$ and from $50°W$ to $50°E$) as well as bands for which the averages overlay almost perfectly. Again, noise induced from the decreased amount of grid boxes for deriving the values is likely to affect the comparison. Both instruments reveal an almost identical vertical distribution of ice clouds (not shown) within the latitude band between $\pm 5°$ where they feature a roughly similar sampling rate. This agreement corroborates the findings of Sellitto et al. (2020).

Figure A1 refers to all ice clouds. For a fair comparison with the CALIPSO data in Figure 1a, i.e. clouds that are (i) flagged as cirrus and (ii) are the only cloud type in the profile, the CATS data set has been screened for what is referred to here as isolated cirrus clouds. The cloud subtype classification is not available in the CATS data set. However, when only ice clouds are present in a profile (i.e., they are not the top of a larger system or part of a mixed-phase system) and these clouds are not flagged as opaque, they are most likely to be cirrus. The CALIPSO Atmospheric_Volume_Description variable and the CATS Percent_Opacity_Fore_FOV variable are used to select clouds that are neither opaque nor fully attenuated.

Figure A2 shows that the vertical profile and the zonal average of the fraction of isolated ice clouds as seen by CATS match those seen by CALIPSO very closely. About 75% to 95% of isolated ice clouds between 7.5 and 17.5 km height are categorised as cirrus. Moreover, 88% of profiles containing isolated ice clouds in CALIPSO data between $51°S$ and $51°N$ are categorised as cirrus (92% for $30°S$ to $30°N$). This fraction decreases towards higher latitudes beyond the area of CATS data coverage between $51°S$ and $51°N$. The findings in Figures A2 suggest that the majority of isolated ice clouds in non-opaque

CATS profiles are equivalent to isolated cirrus in CALIPSO data. In addition, cloud-fraction retrievals for isolated ice clouds in non-opaque profiles give comparable results when using data from the CALIPSO and CATS instruments. As a consequence, the investigation of the diurnal variability of ice clouds considers CATS profiles that contain isolated, non-opaque ice clouds and assumes that these profiles are equivalent to CALIPSO profiles that contain isolated cirrus clouds.

A2 Mid-level clouds

Figure A3 compares the spatial distribution of the occurrence frequency of transparent mid-level clouds as seen by CALIPSO and CATS during the CATS period of operation. Overall, the occurrence frequency is much lower than for ice clouds in Figure A1. In addition, transparent altocumulus is observed primarily over land. Both time series resolve comparable regions of high altocumulus occurrence frequency over southern and eastern Africa, the Middle East, central Asia, western Australia, the Amazon, coastal Peru, and to the west of the Rocky Mountains. Discernible differences are restricted to northern Africa, central Asia, and eastern Australia – all regions where CATS finds a slightly higher altocumulus occurrence frequency than CALIPSO.

Figure A4a shows that the small differences in Figure A3 don't lead to a large deviation in the zonal mean altocumulus fraction. The only exception is visible around 40°N where the higher altocumulus occurrence frequency over western North America and central Asia in CATS observations compared to CALIPSO leads to a higher zonal mean in the CATS data set. The vertical distribution of altocumulus fraction in Figure A4b shows that both instruments place the target clouds within the same height range with a maximum at around 5 km height but a larger altocumulus fraction in the CALIPSO data set compared to the one derived from CATS measurements. As in the case of cirrus in Figure A4b, different absolute maxima in the profiles of cloud fraction from CALIPSO and CATS are most likely the result of slight differences in how these cloud types are inferred from the measurements of the two instruments.

Appendix B: Seasonal and monthly variation

The information in Figure 9 might not be specific enough to consider where to put a ground-based lidar for observing high- and mid-level clouds for a shorter-term field experiment. Seasonally and monthly resolved displays of the data in Figure 9 are therefore presented in Figures A5-A8 to resolve the annual variation in the advantageous conditions for observing altocumulus and cirrus clouds with ground-based lidar.

Author contributions. MT conceived this study and processed and analysed the CALIPSO data. VN processed and analysed the CATS data. Both authors contributed equally to the discussion of the findings, the writing of the paper, and the creation of the figures.

Competing interests. The authors declare no competing interests.

Acknowledgements. This work was supported by the Franco-German Fellowship Programme on Climate, Energy, and Earth System Research (Make Our Planet Great Again – German Research Initiative, MOPGA-GRI) of the German Academic Exchange Service (DAAD), funded by the German Ministry of Education and Research. VN acknowledges funding by CNES and CNRS and would like to thank the IPSL ESPRI and AERIS computation facilities for data storage and analysis capacity. We thank the AERIS/ICARE Data and Services Center (https://www.icare.univ-lille.fr/) for providing access to the data used in this study.

References

320 Adebiyi, A. A., Zuidema, P., Chang, I., Burton, S. P., and Cairns, B.: Mid-level clouds are frequent above the southeast Atlantic stratocumulus clouds, Atmos. Chem. Phys., 20, 11025-11043, https://doi.org/10.5194/acp-20-11025-2020, 2020.

Alexander, S. P. and Klekociuk, A. R.: Constraining ice water content of thin Antarctic cirrus clouds using ground-based lidar and satellite data, J. Atmos. Sci., 78, 1791-1806, https://doi.org/10.1175/JAS-D-20-0251.1, 2021.

Ansmann, A., Wandinger, U., Riebesell, M., Weitkamp, C., and Michaelis, W.: Independent measurement of extinction and
325 backscatter profiles in cirrus clouds by using a combined Raman elastic-backscatter lidar, Appl. Opt., 31, 7113-7131, https://doi.org/10.1364/AO.31.007113, 1992.

Ansmann, A., Mattis, I., Müller, D., Wandinger, U., Radlach, M., Althausen, D., and Damoah, R.: Ice formation in Saharan dust over central Europe observed with temperature/humidity/aerosol Raman lidar, J. Geophys. Res., 110, D18S12, https://doi.org/10.1029/2004JD005000, 2005.

330 Ansmann, A., Tesche, M., Althausen, D., Müller, D., Freudenthaler, V., Heese, B., Wiegner, M., Pisani, G., Knippertz, P., and Dubovik, O.: Influence of Saharan dust on cloud glaciation in southern Morocco during SAMUM, J. Geophys. Res., 113, D04210, https://doi.org/10.1029/2007JD008785, 2008.

Ansmann, A., Tesche, M., Seifert, P., Althausen, D., Engelmann, R., Fruntke, J., Wandinger, U., Mattis, I., and Müller, D.: Evolution of the ice phase in tropical altocumulus: SAMUM lidar observations over Cape Verde, J. Geophys. Res., 114, D17208,
335 https://doi.org/10.1029/2008JD011659, 2009.

Ansmann, A., Mamouri, R.-E., Bühl, J., Seifert, P., Engelmann, R., Hofer, J., Nisantzi, A., Atkinson, J. D., Kanji, Z. A., Sierau, B., Vrekoussis, M., and Sciare, J.: Ice-nucleating particle versus ice crystal number concentration in altocumulus and cirrus layers embedded in Saharan dust: A closure study, Atmos. Chem. Phys., 19, 15087-15115, https://doi.org/10.5194/acp-19-15087-2019, 2019.

Barja Gonzalez, B., Seifert, P., Gouveia, D. A., Zamorano, F., and Rosas, J.: Characterization of cirrus clouds at the southern hemisphere
340 mid-latitude site of Punta Arenas (53°S, 71°W), in AGU Fall Meeting Abstracts, vol. 2020, pp. A033-0012, 2020.

Baumgardner, D., Abel, S. J., Axisa, D., Cotton, R., Crosier, J., Field, P., Gurganus, C., Heymsfield, A., Korolev, A., Krämer, M., Lawson, P., McFarquhar, G., Ulanowski, Z., and Um, J.: Cloud Ice Properties: In situ measurement challenges, Meteorolog. Monogr., 58, 9.1-9.23, https://doi.org/10.1175/AMSMONOGRAPHS-D-16-0011.1, 2017.

Bennartz, R., Shupe, M., Turner, D., Walden, V. P., Steffen, K., Cox, C. J., Kulie, M. S., Miller, N. B., and Pettersen, C.: July 2012 Greenland
345 melt extent enhanced by low-level liquid clouds, Nature, 496, 83-86, https://doi.org/10.1038/nature12002, 2013.

Bourgeois, Q., Ekman, A., Igel, M., and Krejci, R.: Ubiquity and impact of thin mid-level clouds in the tropics, Nat. Commun, 7, 12432, https://doi.org/10.1038/ncomms12432, 2016.

Bühl, J., Alexander, S., Crewell, S., Heymsfield, A., Kalesse, H., Khain, A., Maahn, M., Van Tricht, K., and Wendisch, M.: Remote Sensing, Meteorol. Monogr. 58, 10.1-10.21, https://doi.org/10.1175/AMSMONOGRAPHS-D-16-0015.1, 2017.

350 CALIPSO Cloud Profile Product, https://www-calipso.larc.nasa.gov/resources/calipso_users_guide/data_summaries/profile_data.php (last access: 10 May 2022).

Cloud-Aerosol Transport System (CATS) International Space Station (ISS) Level 2 Operational Night Mode 7.2 Version 3-01 5 km Layer data product, https://doi.org/10.5067/ISS/CATS/L2O_N-M7.2-V3-01_05kmLay (last access: 10 May 2022).

Cloud-Aerosol Transport System (CATS) International Space Station (ISS) Level 2 Operational Night Mode 7.2 Version 3-01 5 km Profile
355 data product, https://doi.org/10.5067/ISS/CATS/L2O_N-M7.2-V3-01_05kmPro (last access: 10 May 2022).

Cheng, C. and Yi, F.: Falling mixed-phase ice virga and their liquid parent cloud layers as observed by ground-based lidars, Remote Sens, 12, 2094, https://doi.org/10.3390/rs12132094, 2020.

Comstock, J. M., Ackerman, T. P., and Mace, G. G.: Ground-based lidar and radar remote sensing of tropical cirrus clouds at Nauru Island: Cloud statistics and radiative impacts, J. Geophys. Res., 107, 4714, https://doi.org/10.1029/2002JD002203, 2002.

360 Dai, G., Wu, S., Song, X., and Liu, L.: Optical and geometrical properties of cirrus clouds over the Tibetan Plateau measured by lidar and radiosonde sounding during the summertime in 2014, Remote Sens., 11, https://doi.org/10.3390/rs11030302, 2019.

Del Guasta, M., Morandi, M., Stefanutti, L., Brechet, J., and Piquad, J.: One year of cloud lidar data from Dumont d'Urville (Antarctica): 1. General overview of geometrical and optical properties, J. Geophys. Res., 98, 18575-18587, https://doi.org/10.1029/93JD01476, 1993.

Dupont, J. C., Haeffelin, M., Morille, Y., Noel, V., Keckhut, P., Winker, D., Comstock, J., Chervet, P., and Roblin, A.: Macrophysical and
365 optical properties of midlatitude cirrus clouds from four ground-based lidars and collocated CALIOP observations, J. Geophys. Res., 115, D00H24, https://doi.org/10.1029/2009JD011943, 2010.

Giannakaki, E., Balis, D. S., Amiridis, V., and Kazadzis, S.: Optical and geometrical characteristics of cirrus clouds over a Southern European lidar station, Atmos. Chem. Phys., 7, 5519-5530, https://doi.org/10.5194/acp-7-5519-2007, 2007.

Gedzelman, S. D.: In Praise of Altocumulus, Weatherwise, 41, 143-149, https://doi.org/10.1080/00431672.1988.9930533, 1988.

370 Gouveia, D. A., Barja, B., Barbosa, H. M. J., Seifert, P., Baars, H., Pauliquevis, T., and Artaxo, P.: Optical and geometrical proper-
ties of cirrus clouds in Amazonia derived from 1 year of ground-based lidar measurements, Atmos. Chem. Phys., 17, 3619-3636, https://doi.org/10.5194/acp-17-3619-2017, 2017.

Haarig, M., Engelmann, R., Ansmann, A., Veselovskii, I., Whiteman, D. N., and Althausen, D.: 1064-nm rotational Raman lidar for particle extinction and lidar-ratio profiling: Cirrus case study, Atmos. Meas. Tech., 9, 4269-4278, https://doi.org/10.5194/amt-9-4269-2016, 2016.

375 He, Q. S., Li, C. C., Ma, J. Z., Wang, H. Q., Shi, G. M., Liang, Z. R., Luan, Q., Geng, F. H., and Zhou, X. W.: The properties and formation of cirrus clouds over the Tibetan Plateau based on summertime lidar measurements, J. Atmos. Sci., 70, 901-915, https://doi.org/10.1175/JAS-D-12-0171.1, 2013.

Heymsfield, A. J., Krämer, M., Luebke, A., Brown, P., Cziczo, D. J., Franklin, C., Lawson, P., Lohmann, U., McFarquhar, G., Ulanowski, Z., and Van Tricht, K.: Cirrus Clouds, Meteorolog. Monogr., 58, 2.1-2.26 , https://doi.org/10.1175/AMSMONOGRAPHS-D-16-0010.1,
380 2017.

Hoareau, C., Keckhut, P., Noel, V., Chepfer, H., and Baray, J.-L.: A decadal cirrus clouds climatology from ground-based and spaceborne lidars above the south of France (43.9° N – 5.7° E), Atmos. Chem. Phys., 13, 6951-6963, https://doi.org/10.5194/acp-13-6951-2013, 2013.

Hong, Y. and Liu, G.: The characteristics of ice cloud properties derived from CloudSat and CALIPSO measurements, J. Clim., 28(9),
385 3880-3901, https://doi.org/10.1175/JCLI-D-14-00666.1, 2015.

Jimenez, C., Ansmann, A., Engelmann, R., Donovan, D., Malinka, A., Seifert, P., Wiesen, R., Radenz, M., Yin, Z., Bühl, J., Schmidt, J., Barja, B., and Wandinger, U.: The dual-field-of-view polarization lidar technique: A new concept in monitoring aerosol effects in liquid-water clouds – case studies, Atmos. Chem. Phys., 20, 15265-15284, https://doi.org/10.5194/acp-20-15265-2020, 2020.

Kanitz, T., Seifert, P., Ansmann, A., Engelmann, R., Althausen, D., Casiccia, C., and Rohwer, E. G.: Contrasting the im-
390 pact of aerosols at northern and southern midlatitudes on heterogeneous ice formation, Geophys. Res. Lett., 38, L17802, https://doi.org/10.1029/2011GL048532, 2011.

Kienast-Sjögren, E., Rolf, C., Seifert, P., Krieger, U. K., Luo, B. P., Krämer, M., and Peter, T.: Climatological and radiative properties of midlatitude cirrus clouds derived by automatic evaluation of lidar measurements, Atmos. Chem. Phys., 16, 7605-7621, https://doi.org/10.5194/acp-16-7605-2016, 2016.

395 Korolev, A., McFarquhar, G., Field, P. R., Franklin, C., Lawson, P., Wang, Z., Williams, E., Abel, S. J., Axisa, D., Borrmann, S., Crosier, J., Fugal, J., Krämer, M., Lohmann, U., Schlenczek, O., Schnaiter, M., and Wendisch, M.: Mixed-Phase Clouds: Progress and Challenges, Meteorolog. Monogr., 58, 5.1-5.50, https://doi.org/10.1175/AMSMONOGRAPHS-D-17-0001.1, 2017.

Lacour, A., Chepfer, H., Miller, N. B., Shupe, M. D., Noel, V., Fettweis, X., Gallee, H., Kay, J. E., Guzman, R., and Cole, J.: How well are clouds simulated over Greenland in climate models? Consequences for the surface cloud radiative effect over the ice sheet, J. Clim., 31,
400 9293-9312, https://doi.org/10.1175/JCLI-D-18-0023.1, 2018.

Liu, Z., Omar, A. H., Hu, Y., Vaughan, M. A., and Winker, D. M.: CALIOP algorithm theoretical basis document—Part 3: Scene classification algorithms. Release 1.0, PC-SCI-202, NASA Langley Research Center, Hampton, VA, 56 pp., available at http://www-calipso.larc.nasa.gov/resources/pdfs/PC-SCI-202_Part3_v1.0.pdf (last access: 13 December 2021), 2005.

Liu, Z., Vaughan, M., Winker, D., Kittaka, C., Getzewich, B., Kuehn, R., Omar, A., Powell, K., Trepte, C., and Hostetler, C.: The CALIPSO
405 lidar cloud and aerosol discrimination: Version 2 algorithm and initial assessment of performance, J. Atmos. Ocean. Tech., 26, 1198-1213, 2009.

McGill, M. J., Yorks, J. E., Scott, V. S., Kupchock, A. W., and Selmer, P. A.: The Cloud-Aerosol Transport System (CATS): A technology demonstration on the International Space Station, Proc. Spie., 9612, 96120A, https://doi.org/10.1117/12.2190841, 2015.

Noel, V., Chepfer, H., Chiriaco, M., and Yorks, J.: The diurnal cycle of cloud profiles over land and ocean between 51° S and 51° N, seen
410 by the CATS spaceborne lidar from the International Space Station, Atmos. Chem. Phys., 18, 9457-9473, https://doi.org/10.5194/acp-18-9457-2018, 2018.

Pandit, A. K., Gadhavi, H. S., Venkat Ratnam, M., Raghunath, K., Rao, S. V. B., and Jayaraman, A.: Long-term trend analysis and climatology of tropical cirrus clouds using 16 years of lidar data set over Southern India, Atmos. Chem. Phys., 15, 13833-13848, https://doi.org/10.5194/acp-15-13833-2015, 2015.

415 Pauly, R. M., Yorks, J. E., Hlavka, D. L., McGill, M. J., Amiridis, V., Palm, S. P., Rodier, S. D., Vaughan, M. A., Selmer, P. A., Kupchock, A. W., Baars, H., and Gialitaki, A.: Cloud-Aerosol Transport System (CATS) 1064 nm calibration and validation, Atmos. Meas. Tech., 12, 6241-6258, https://doi.org/10.5194/amt-12-6241-2019, 2019.

Pitts, M. C., Poole, L. R., and Gonzalez, R.: Polar stratospheric cloud climatology based on CALIPSO spaceborne lidar measurements from 2006 to 2017, Atmos. Chem. Phys., 18, 10881-10913, https://doi.org/10.5194/acp-18-10881-2018, 2018.

420 Platt, C.M.R.: Lidar and radiometric observations of cirrus clouds, J. Atmos. Sci., 30, 1191-1204, https://doi.org/10.1175/1520-0469(1973)030<1191:LAROOC>2.0.CO;2, 1973.

Platt, C.M.R.: Remote sounding of high clouds: I. Calculation of visible and infrared optical properties from lidar and radiometer measurements, J. Appl. Meteorol. Clim., 18(9), 1130-1143, https://doi.org/10.1175/1520-0450(1979)018<1130:RSOHCI>2.0.CO;2, 1979.

Protat, A., Delanoë, J., Plana-Fattori, A., May, P. T. and O'Connor, E. J.: The statistical properties of tropical ice clouds generated
425 by the West African and Australian monsoons, from ground-based radar–lidar observations. Q. J. R. Meteorol. Soc., 136, 345-363, https://doi.org/10.1002/qj.490, 2010.

Protat, A., Delanoë, J., May, P. T., Haynes, J., Jakob, C., O'Connor, E., Pope, M., and Wheeler, M. C.: The variability of tropical ice cloud properties as a function of the large-scale context from ground-based radar-lidar observations over Darwin, Australia, Atmos. Chem. Phys., 11, 8363-8384, https://doi.org/10.5194/acp-11-8363-2011, 2011.

430   Radenz, M., Bühl, J., Seifert, P., Baars, H., Engelmann, R., Barja González, B., Mamouri, R.-E., Zamorano, F., and Ansmann, A.: Hemispheric contrasts in ice formation in stratiform mixed-phase clouds: Disentangling the role of aerosol and dynamics with ground-based remote sensing, Atmos. Chem. Phys., 21, 17969-17994, https://doi.org/10.5194/acp-21-17969-2021, 2021.

Sassen, K. and Cho, B. S.: Subvisual-thin cirrus lidar dataset for satellite verification and climatological research, J. Appl. Meteorol. Clim., 31(11), 1275-1285, https://doi.org/10.1175/1520-0450(1992)031<1275:STCLDF>2.0.CO;2, 1992.

435   Sassen, K. and Campbell, J. R.: A Midlatitude cirrus cloud climatology from the Facility for Atmospheric Remote Sensing. Part I: Macrophysical and synoptic properties, J. Atmos. Sci., 58(5), 481-496, https://doi.org/10.1175/1520-0469(2001)058<0481:AMCCCF>2.0.CO;2, 2001.

Sassen, K., and Benson, S.: A Midlatitude cirrus cloud climatology from the Facility for Atmospheric Remote Sensing. Part II: Microphysical properties derived from lidar depolarization, J. Atmos. Sci., 58(15), 2103-2112, https://doi.org/10.1175/1520-
440   0469(2001)058<2103:AMCCCF>2.0.CO;2, 2001.

Sassen, K.: Indirect climate forcing over the western US from Asian dust storms, Geophys. Res. Lett., 29, https://doi.org/10.1029/2001GL014051, 2002.

Schmidt, J., Ansmann, A., Bühl, J., and Wandinger, U.: Strong aerosol–cloud interaction in altocumulus during updraft periods: lidar observations over central Europe, Atmos. Chem. Phys., 15, 10687-10700, https://doi.org/10.5194/acp-15-10687-2015, 2015.

445   Seifert, P., Ansmann, A., Müller, D., Wandinger, U., Althausen, D., Heymsfield, A. J., Massie, S. T., and Schmitt, C.: Cirrus optical properties observed with lidar, radiosonde, and satellite over the tropical Indian Ocean during the aerosol-polluted northeast and clean maritime southwest monsoon, J. Geophys. Res., 112, D17205, https://doi.org/10.1029/2006JD008352, 2007.

Seifert, P., Ansmann, A., Mattis, I., Wandinger, U., Tesche, M., Engelmann, R., Müller, D., Pérez, C., and Haustein, K.: Saharan dust and heterogeneous ice formation: eleven years of cloud observations at a central European EARLINET site, J. Geophys. Res., 115, D20201,
450   https://doi.org/10.1029/2009JD013222, 2010.

Seifert, P., Ansmann, A., Groß, S., Freudenthaler, V., Heinold, B., Hiebsch A., Mattis, I., Schmidt, J., Schnell, F., Tesche, M., Wandinger, U., and Wiegner, M.: Ice formation in ash-influenced clouds after the eruption of the Eyjafjallajökull volcano in April 2010, J. Geophys. Res., 116, D00U04, https://doi.org/10.1029/2011JD015702, 2011.

Seifert, P., Kunz, C., Baars, H., Ansmann, A., Bühl, J., Senf, F., Engelmann, R., Althausen, D., and Artaxo, P.: Seasonal vari-
455   ability of heterogeneous ice formation in stratiform clouds over the Amazon Basin, Geophys. Res. Lett., 42, 5587–5593, https://doi.org/10.1002/2015GL064068, 2015.

Sellitto, P., Bucci, S., and Legras, B.: Comparison of ISS–CATS and CALIPSO–CALIOP characterization of high clouds in the Tropics, Remote Sens., 12, 3946, https://doi.org/10.3390/rs12233946, 2020.

Solomon, A., Shupe, M. D., and Miller, N. B.: Cloud-atmospheric boundary layer-surface interactions on the Greenland Ice Sheet during the
460   July 2012 extreme melt event, J. Clim., 30, 3237-3252, https://doi.org/10.1175/JCLI-D-16-0071.1, 2017.

Tesche, M., Achtert, P., and Pitts, M. C.: On the best locations for ground-based polar stratospheric cloud (PSC) observations, Atmos. Chem. Phys., 21, 505–516, https://doi.org/10.5194/acp-21-505-2021, 2021.

Winker, D. M., Vaughan, M. A., Omar, A., Hu, Y., Powell, K. A., Liu, Z., Hunt, W. H., and Young, S. A.: Overview of the CALIPSO mission and CALIOP data processing algorithms, J. Atmos. Ocean. Techn., 26, 2310-2323, https://doi.org/10.1175/2009JTECHA1281.1, 2009.

465   Winker, D. M., Tackett, J. L., Getzewich, B. J., Liu, Z., Vaughan, M. A., and Rogers, R. R.: The global 3-D distribution of tropospheric aerosols as characterized by CALIOP, Atmos. Chem. Phys., 13, 3345-3361, https://doi.org/10.5194/acp-13- 3345-2013, 2013.

Yi, Y., Yi, F., Liu, F., Zhang, Y., Yu, C., and He, Y.: Microphysical process of precipitating hydrometeors from warm-front mid-level stratiform clouds revealed by ground-based lidar observations, Atmos. Chem. Phys., 21, 17649-17664, https://doi.org/10.5194/acp-21-17649-2021, 2021.

470 Yorks, J. E., Hlavka D. L., Vaughan, M. A., McGill, M. J., Hart, W. D., Rodier, S. D., and Kuehn, R. E.: Airborne validation of cirrus cloud properties derived from CALIPSO lidar measurements: Spatial properties, J. Geophys. Res.: Atmos., 116, D19207, https://doi.org/10.1029/2011JD015942, 2011.

Yorks, J. E., McGill, M. J., Palm, S. P., Hlavka, D. L., Selmer, P. A., Nowottnick, E. P., Vaughan, M. A., Rodier, S. D., and Hart, W. D.: An overview of the CATS level 1 processing algorithms and data products, Geophys. Res. Lett., 43, 4632–4639,

475 https://doi.org/10.1002/2016GL068006, 2016a.

Yorks, J. E., Palm, S. P., McGill, M. J., Hlavka, D. L., Hart, W. D., Selmer, P. A., and Nowottnick, E.: CATS Algorithm Theoretical Basis Document, Level 1 and Level 2 Data Products, release 1.2, available at https://cats.gsfc.nasa.gov/media/docs/CATS_ATBD.pdf (last access: 10 May 2022), 2016b.
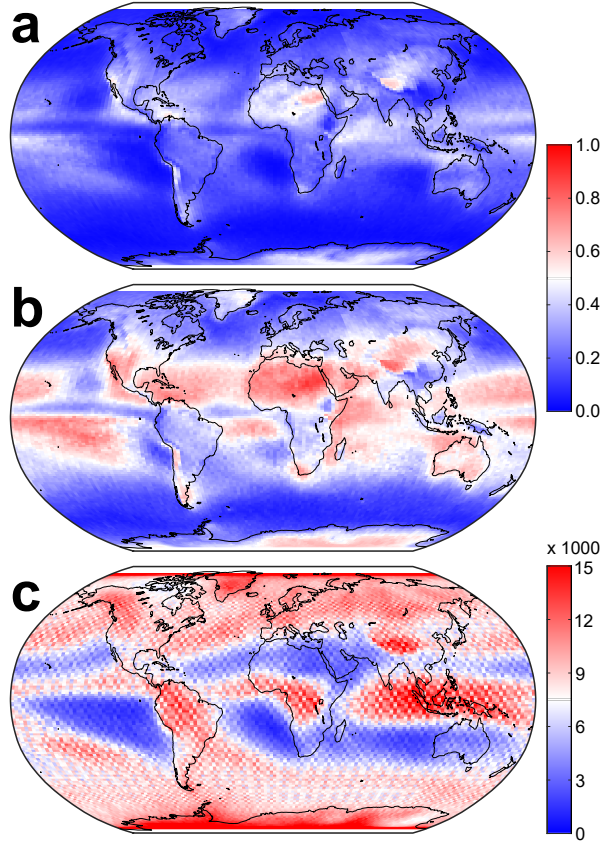
Figure 1. Global distribution of (a) the ratio of CALIPSO profiles that contain cirrus clouds in the absence of opaque low- and mid-level clouds versus all cloudy profiles, (b) the ratio of CALIPSO profiles that contain cirrus clouds in the absence of opaque low- and mid-level clouds versus all cirrus-containing cloudy profiles, and (c) the number of cirrus-containing cloudy profiles per grid box.

Table 1. Number of considered CALIOP cloud profiles per category. Ac refers to transparent altocumulus. Ci only and Ac only refer to those profiles in which the view of the respective cloud type from the ground would not be distorted by the absence of opaque clouds underneath.

category	all	cloudy	cloudy with Ci	cloudy with Ac	Ci only	Ac only
all	569,254,944	348,685,952	164,447,440	79,403,704	59,082,728	45,334,236
day	282,916,480	182,175,776	72,997,168	38,924,668	25,370,064	22,130,464
night	249,142,704	166,510,144	80,447,224	40,479,040	29,892,528	23,203,772
DJF	139,831,131	90,198,264	38,025,076	21,086,660	13,265,246	11,913,064
MAM	142,231,878	92,319,760	41,793,772	22,006,846	15,396,790	12,573,698
JJA	144,220,790	95,928,208	43,420,960	20,742,324	16,048,742	12,288,093
SON	142,971,145	94,792,768	41,207,624	21,309,664	14,371,952	11,787,976
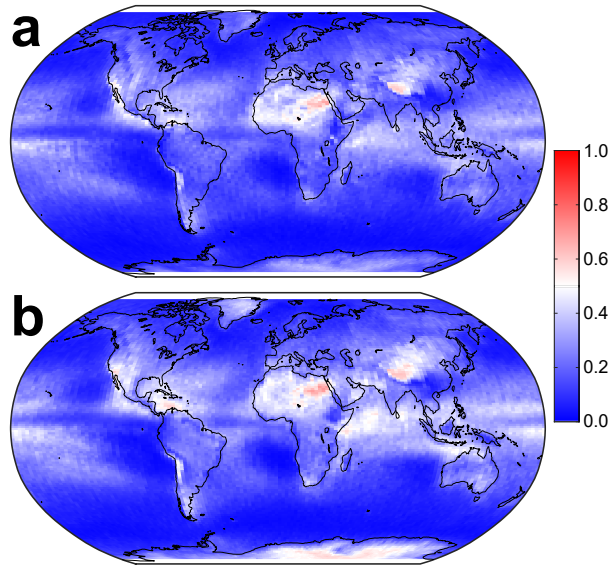
Figure 2. Same as Figure 1a but separated according to CALIPSO observations during (a) day and (b) night.
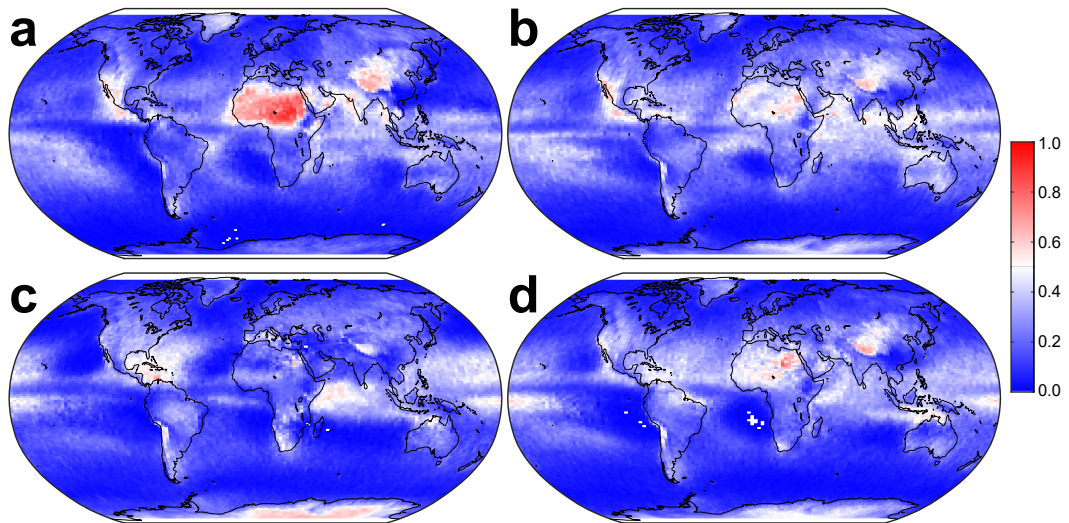
Figure 3. Same as Figure 1a but for the three-month periods (a) DJF, (b) MAM, (c) JJA, and (d) SON.
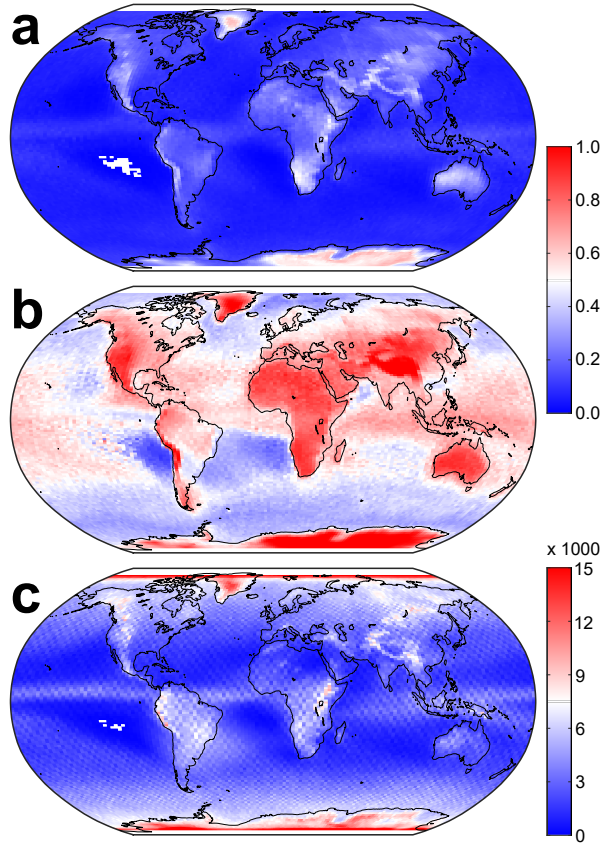
Figure 4. Global distribution of (a) the ratio of CALIPSO profiles that contains transparent altocumulus in the absence of opaque low-level clouds versus all cloudy profiles, (b) the ratio of CALIPSO profiles that contain transparent altocumulus in the absence of opaque low-level clouds versus all cloudy profiles that contain this cloud type, and (c) the number of cloudy profiles per grid box that contain altocumulus transparent.
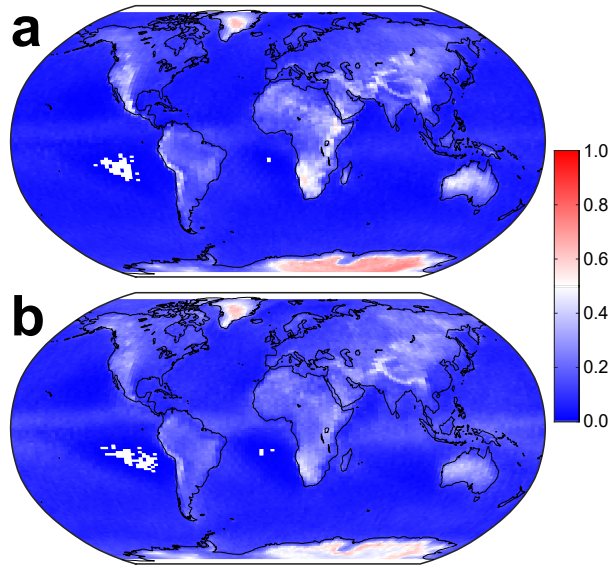
Figure 5. Same as Figure 4a but separated according to CALIPSO observations during (a) day and (b) night.
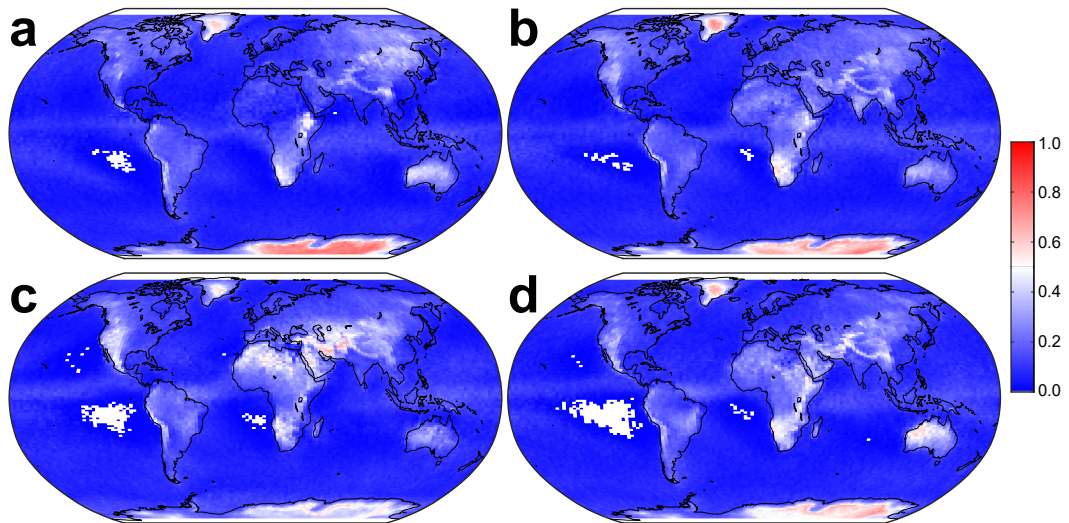
Figure 6. Same as Figure 4a but for the three-month periods (a) DJF, (b) MAM, (c) JJA, and (d) SON.
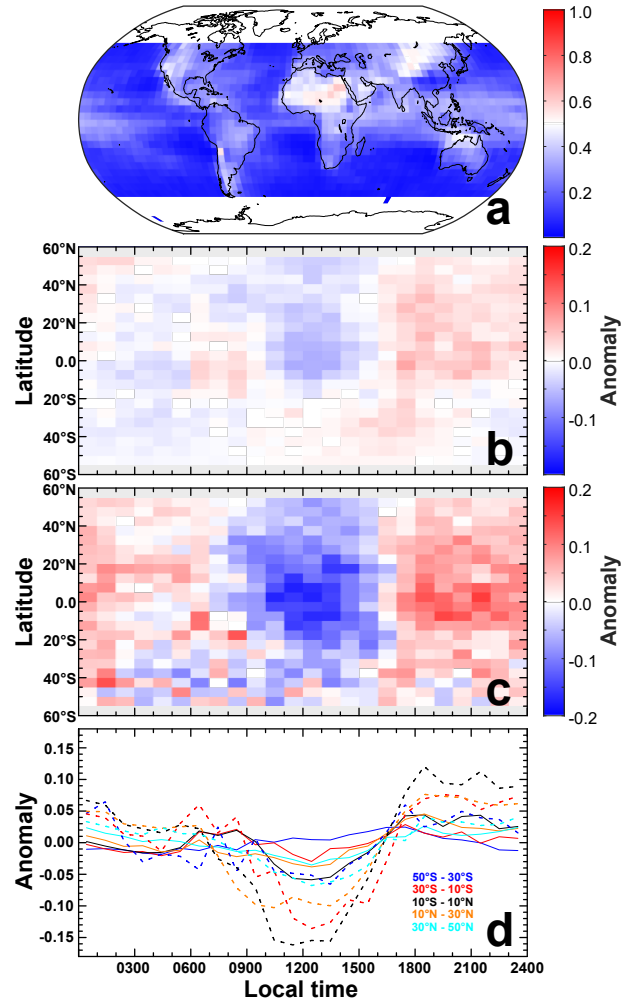
Figure 7. Occurrence rate of isolated ice clouds in CATS observations between March 2015 and October 2017 as (a) global distribution, (b and c) anomaly in the diurnal variation of the zonal distribution over all surfaces and land only, and (d) anomaly in the diurnal variation of the zonal average in five latitude bands: 50°S–30°S (blue), 30°S–10°S (red), 10°S–10°N (black), 10°N–30°N (orange), and 30°N–50°N (light blue) over all surfaces (solid) and land only (dashed). The anomaly is calculated as the difference between hourly values and the daily mean value.
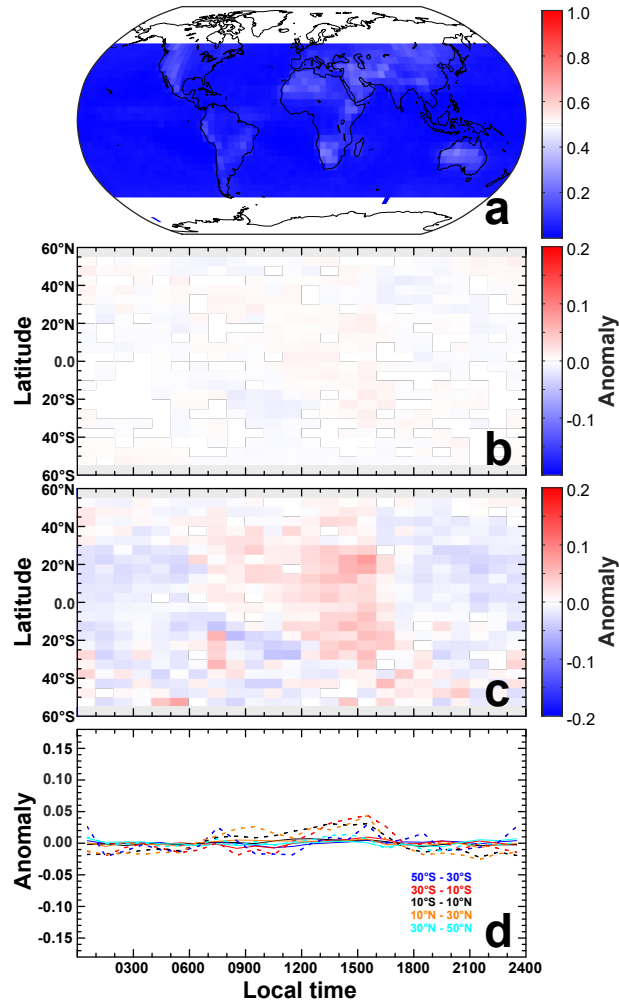
Figure 8. Occurrence rate of isolated mid-level clouds in CATS observations between March 2015 and October 2017 as (a) global distribution, (b and c) anomaly in the diurnal variation of the zonal distribution over all surfaces and land only, and (d) anomaly in the diurnal variation of the zonal average in five latitude bands: 50°S–30°S (blue), 30°S–10°S (red), 10°S–10°N (black), 10°N–30°N (orange), and 30°N–50°N (light blue) over all surfaces (solid) and land only (dashed). The anomaly is calculated as the difference between hourly values and the daily mean value.
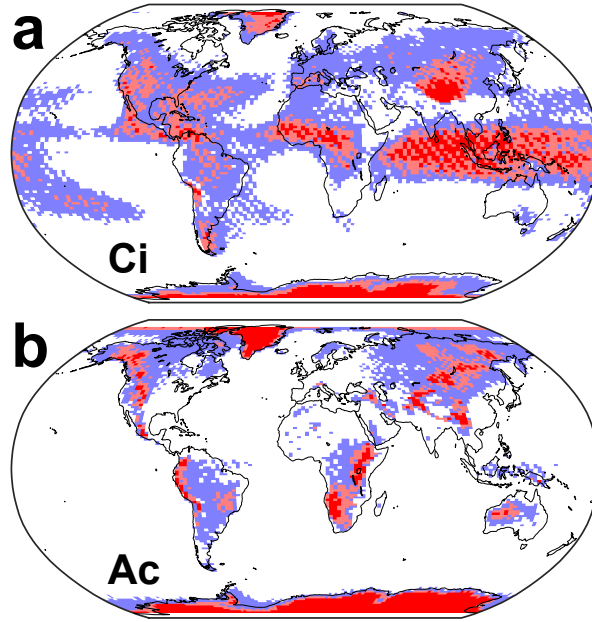
Figure 9. Overview of the best regions for placing a ground-based lidar for observing (a) high and (b) mid-level clouds derived from multiplying the data in Figures 1a and 4a with the normalised number of profiles per grid box, i.e. Figure 1c divided by 33955 and Figure 4c 27469, respectively. The colours refer to the factors for meeting suitable conditions for ground-based lidar observations of the two cloud types. For cirrus clouds, the colours mark the ranges 0.0000 to 0.0399 (white), 0.0400 to 0.0799 (light blue), 0.0800 to 0.1199 (light red), and >0.1200 (red). The corresponding ranges for altocumulus clouds are 0.0000 to 0.0249, 0.0250 to 0.0499, 0.0500 to 0.0749, and >0.0750.
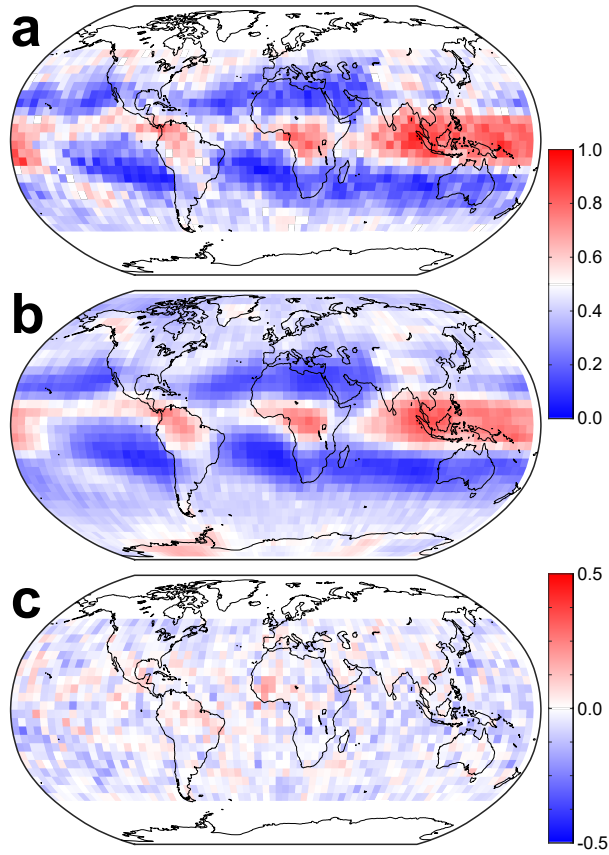
Figure A1. Global distribution of the fraction of cirrus clouds in observations with the (a) CATS and (b) CALIPSO lidars and (c) difference between CALIPSO and CATS for the time period from March 2015 to October 2017. Only CATS data within ±1 hour around the fixed CALIPSO overpass times are considered.
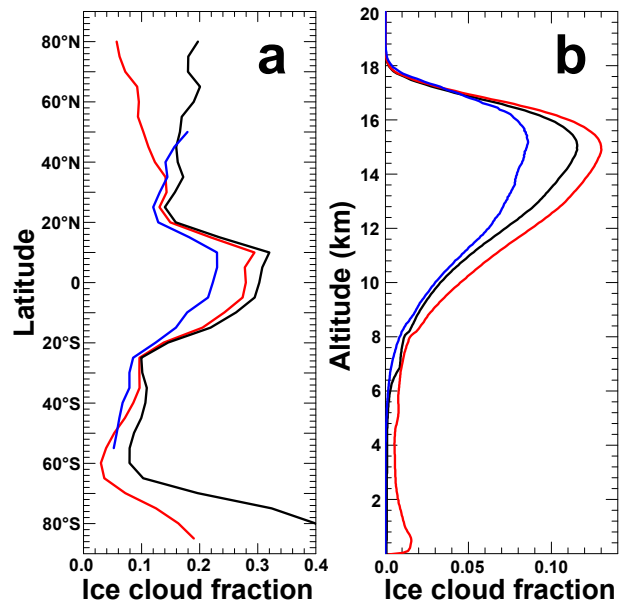
Figure A2. (a) Latitudinal distribution and (b) height profiles of the cloud fractions of isolated cirrus as seen by CALIPSO (black) and of isolated ice clouds as seen by CALIPSO (red) and CATS (blue) for the time period from March 2015 to October 2017.
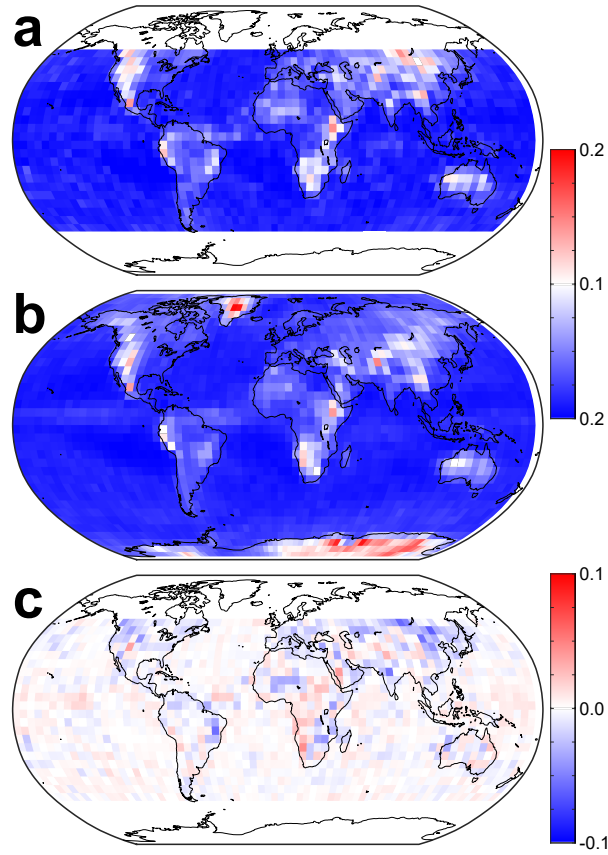
Figure A3. Global distribution of the fraction of mid-level clouds in observations with the (a) CATS and (b) CALIPSO lidars and (c) difference between CALIPSO and CATS for the time period from March 2015 to October 2017. Only CATS data within ± 1 hour around the fixed CALIPSO overpass times are considered.
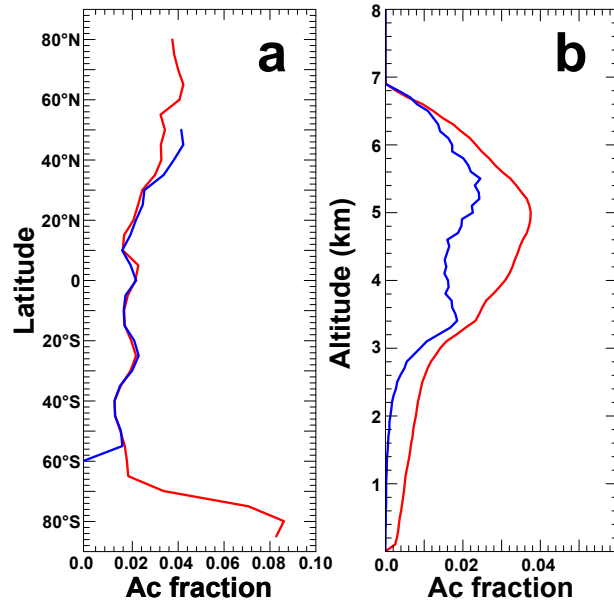
Figure A4. (a) Latitudinal distribution and (b) height profiles of the altocumulus cloud fraction as seen by CALIPSO (red) and CATS (blue) for the time period from March 2015 to October 2017.
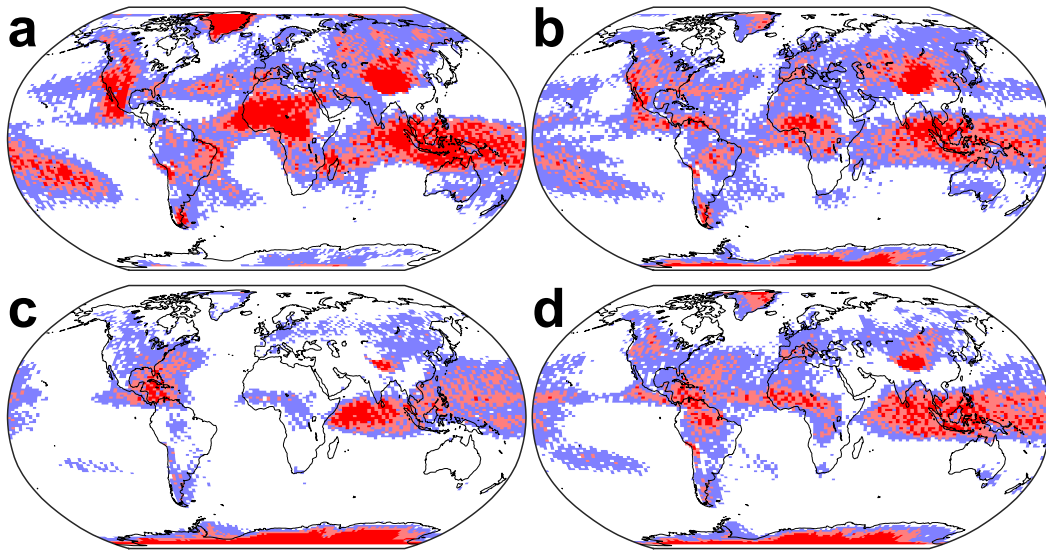
Figure A5. Same as Figure 9a but for the three-month periods (a) DJF, (b) MAM, (c) JJA, and (d) SON.
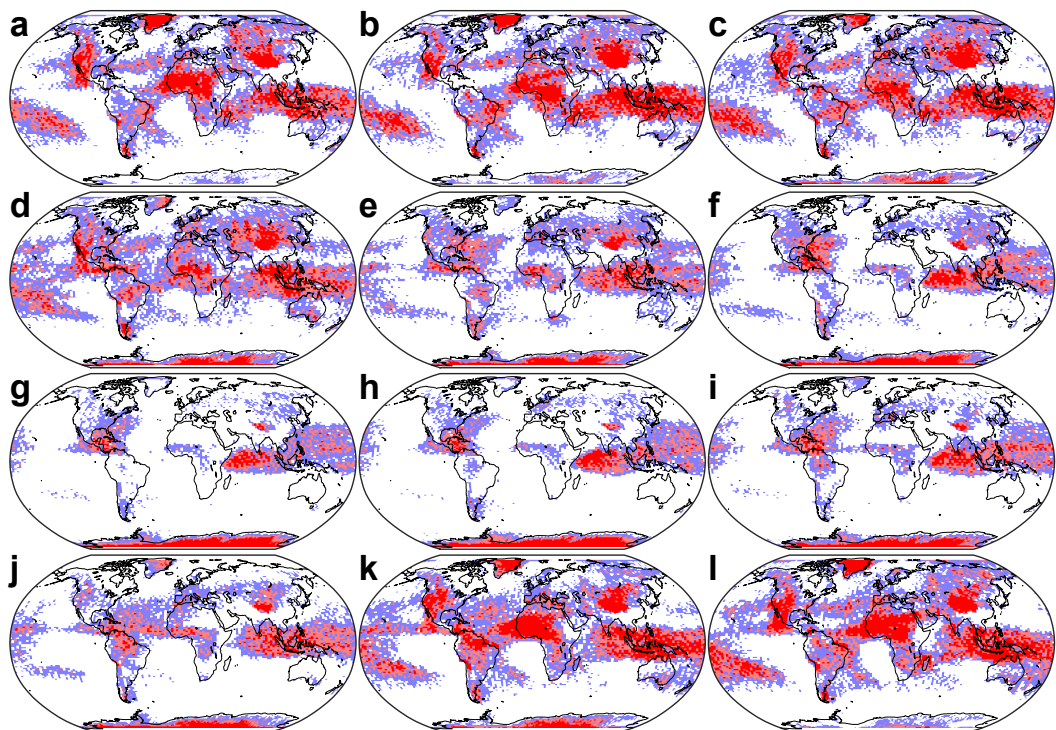
Figure A6. Same as Figure 9a but for individual months: (a) January, (b) February, (c) March, (d) April, (e) May, (f) June, (g) July, (h) August, (i) September, (j) October, (k) November, and (l) December.
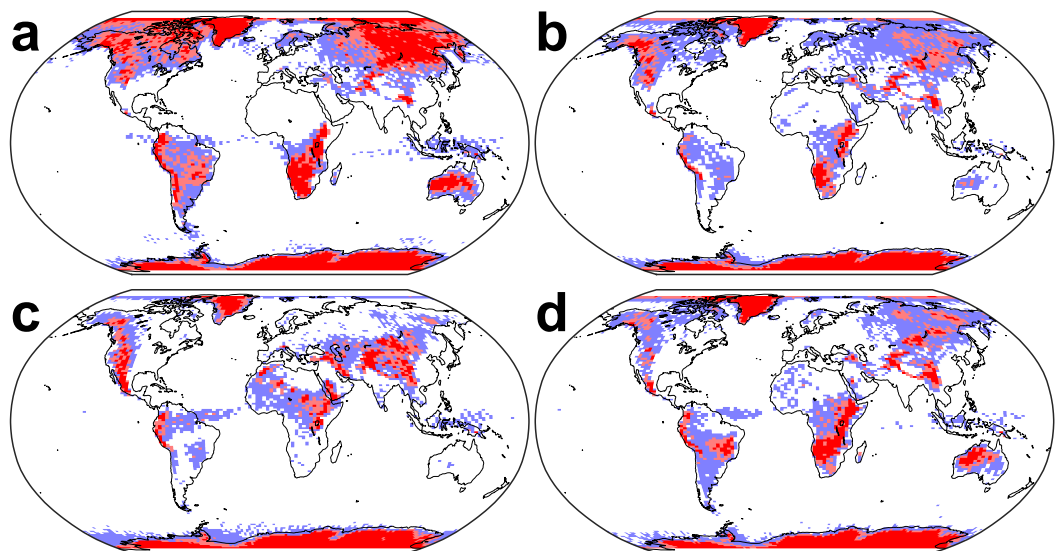
Figure A7. Same as Figure 9b but for the three-month periods (a) DJF, (b) MAM, (c) JJA, and (d) SON.
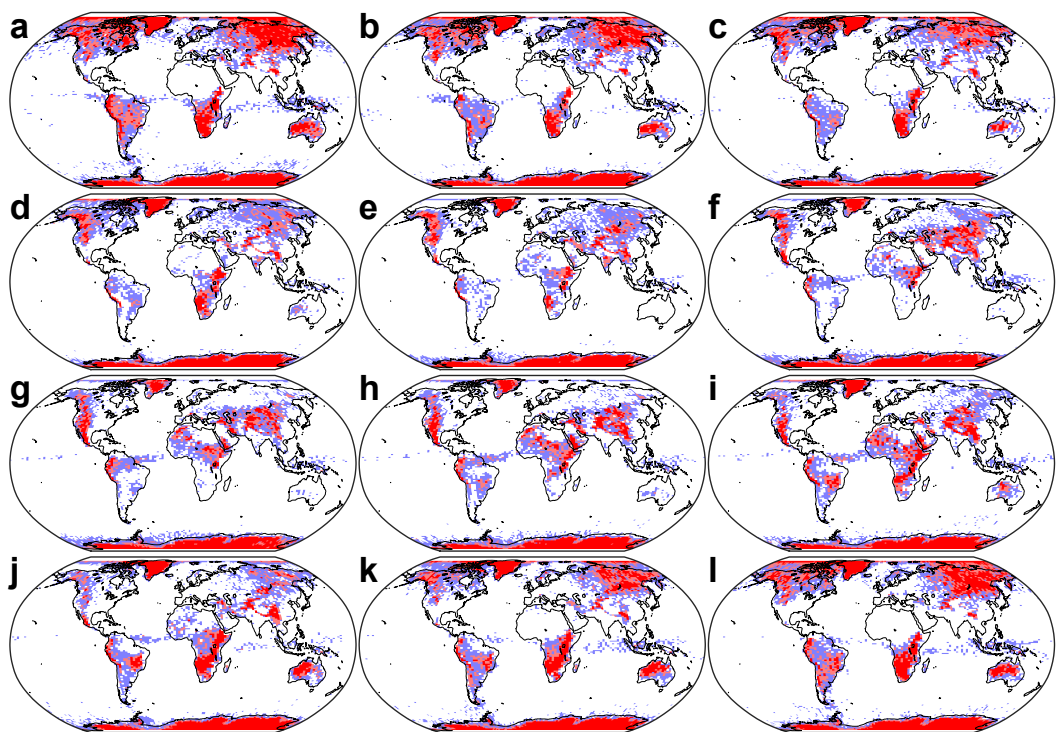
Figure A8. Same as Figure 9b but for individual months: (a) January, (b) February, (c) March, (d) April, (e) May, (f) June, (g) July, (h) August, (i) September, (j) October, (k) November, and (l) December.